International Journal of Power Electronics and Drive System (IJPEDS)
Vol. 17, No. 3, September 2026, pp. 1620∼1629
ISSN: 2088-8694, DOI: 10.11591/ijpeds.v17.i3.pp1620-1629

Lyapunov controller design for a fuel cell electric vehicle powered by a three-level floating capacitor boost converter

Chaouqi Aouadi[1,2], Abdelmajid Abouloifa[1], Meriem Aourir[3], Ibtissam Lachkar[1]
[1]ESE Lab, ENSEM of Casablanca, University Hassan II, Casablanca, Morocco
[2]Department of Electrical Engineering, ENSEM of Casablanca, University Hassan II, Casablanca, Morocco
[3]LIME Lab, ISGA Casablanca, Edvantis Higher Education, Casablanca, Morocco

Article Info

Article history:

Received Aug 9, 2025
Revised Mar 24, 2026
Accepted Apr 23, 2026

Keywords:

Boost converter
Electric vehicle
Flying capacitor
Lyapunov theorem
Nonlinear controller
Stability analysis

ABSTRACT

Electric vehicles (EVs) have undergone considerable progress facilitated by the adoption of contemporary technologies, such as innovative energy sources like the fuel cell (FC) in conjunction with novel power converter architectures. In this context, this work addresses the problem of controlling a three-level flying capacitor boost converter (FCBC) powered by a fuel cell. The converter is linked at its output to an impedance modelling the DC/AC converter and a brushless motor integrated into an FC-EV. Variations in load demand and power provided by the fuel cell are an issue to be considered, alongside voltage balancing, which involves maintaining balanced voltages between flying capacitors, as an imbalance can lead to uneven component voltage and reduced converter efficiency. To solve these issues, a nonlinear controller is developed making use of the Lyapunov approach which ensures the proper operation of the system by continuously adjusting control actions based on the system dynamics. Indeed, the regulator comprises three loops: one dedicated to balancing the voltage across the flying capacitor, and two nested loops; The inner loop controls the inductor current, while the outer loop regulates the output voltage.

Corresponding Author:

Chaouqi Aouadi
ESE Lab, ENSEM of Casablanca, University Hassan II
Casablanca, Morocco
Email: chaouqi.aouadi@univh2c.ma

1. INTRODUCTION

Sustainable energy sources, including photovoltaic (PV) energy and hydrogen energy, have become a crucial element in social development. The need for clean energy-based systems is currently growing considerably [1]–[3], particularly in key sectors such as industry and transport. The latter has undergone a remarkable evolution with the deployment of electric vehicles (EV), replacing conventional internal combustion engine vehicles known for their substantial emissions of greenhouse gases. Electric vehicles are systematically categorized based on the specific energy source that powers their drive system [4]. When the automobile is powered exclusively by a battery, it is referred to as a battery electric vehicle (BEV). If, in addition to the battery, the electric vehicle incorporates a fuel cell or internal combustion engine, it is classified as a fuel cell electric vehicle (FCEV) or hybrid electric vehicle (HEV), respectively. Energy source, drivetrain system, and power electronics with its control unit are the essential parts of an EV [5]. Fuel cell (FC) is one of the energy sources being promoted to be used alongside the batteries in FCEV. The voltage supplied by proton exchange membrane fuel cells (PEMFCs) integrated into EVs is relatively low. To overcome this issue, a

DC/DC conversion interface was added to increase the power at the terminals of the FC [6]. Many DC/DC converter topologies are studied in the literature [7]–[10], and they can be categorized into two groups. The first group comprises classical converters such as the boost converter and the buck converter. The second class includes multilevel power converters [9], [11], which offer a high voltage gain [12]–[14] without using a high duty cycle.

This paper focuses on the study of the integration of a three-stage flying capacitor boost converter (FCBC) [15]–[17] in a fuel cell electric vehicle. The FCBC is a variant of a multi-level boost converter that offers several advantages compared with a conventional boost chopper [17]. One of the key benefits is a significant increase in voltage amplification due to the floating capacitor that stores energy and contributes to the amplification and transfer of energy from a PEMFC source to the load. It also offers a small input inductance, which contributes to reducing its size [18].

The FCBC is suitable for adapting current and voltage levels from a low-voltage source, but its control remains a challenge due to the zero dynamics [19]. Alongside regulating the FCBC output voltage, it is important to consider stabilizing the floating capacitor voltage. Inadequate stabilization results in high voltage stress across power switches and increased power losses [15]. To address this issue, several methods for stabilizing floating capacitor voltage have been proposed [19]–[22]. The primary purpose of this paper is to propose a controller for a three-level FCBC used in FCEV that achieves two objectives:

– CO1: controlling the voltage across the load; this objective is accomplished through two cascaded loops: an internal loop regulates the inductor current while an external loop controls the output voltage.
– CO2: stabilizing the flying capacitor voltage; this objective is realized using a single control loop that enforces the flying capacitor voltage to follow its reference. This study contributes to the literature as follows: i) Designing a nonlinear controller based on large signal non-linear model, unlike other works that use linear methods for system modeling and controller synthesis [17]; and ii) The global stability of the system is demonstrated by mathematical tools and validated numerically by simulations, which confirm the robustness and effectiveness of the controllers against disturbances and load variation.

The remaining part of this work is organized as follows: i) The second section focuses on system description and mathematical modeling; ii) Section 3 is dedicated to controller design; iii) Section 4 is devoted to stability analysis; iv) A simulation was then carried out to validate the controller's effectiveness in section 5; and v) A conclusion at the end of the paper.

2. SYSTEM DESCRIPTION AND MODELLING

The hybrid vehicle shown in Figure 1 can be driven by two energy chains [23] and [24]. The first consists of a lithium battery associated with a bidirectional DC/DC converter, while second consists of a fuel cell connected to a three-level boost converter presented in Figure 2. Both energy sources can provide power to the vehicle's drive system, which consists of a DC/AC converter and a brushless motor. The fuel cell-boost converter association is subject of the study presented in this work. Indeed, from a topological point of view, the boost converter used in this study considerably reduces the voltage stress on the semiconductors, while from a control point of view, the system presents a challenge due to its complex, non-linear, and hybrid model.

2.1. Three level FCBC modelling

Figure 2 illustrates the diagram of three-level boost converter, powered by a fuel cell and supplying an impedance Z_L which is the downstream circuit formed by the brushless motor-converter combination. The circuit includes two unidirectional current semiconductors $(D_1,\ D_2)$ with spontaneous switching and two bidirectional current semiconductors $(S_1,\ S_2)$ with controlled switching by two binary signals $(\mu_1,\ \mu_2)$ which are generated by phase shifted PWM (PSPWM) strategy.

The converter dynamics is represented by the well-known average model (1)–(3). where v_{in}, i_L, v_c and v_o denote respectively, input voltage, current through inductance L, the voltage across floating capacitor C and output voltage. The signals (μ_1, μ_2) are the switched control inputs. Control law is developed on the basis of the model given in the (4)–(6), by respecting the following variable change; $x_1 = i_L$, $x_2 = v_c$ and $x_3 = v_o$.

$$L\dot{x}_1 = v_{in} + (u_1 - u_2)\, x_2 - (1 - u_2)\, x_3 \tag{1}$$

$$C\dot{x}_2 = -\left(u_1 - u_2\right) x_1 \tag{2}$$

$$C_o\dot{x}_3 = -i_Z + \left(1 - u_2\right) x_1 \tag{3}$$

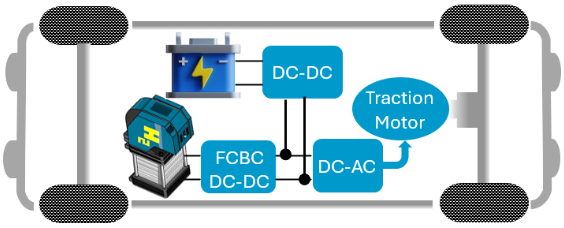

Figure 1. Fuel cell electric vehicle

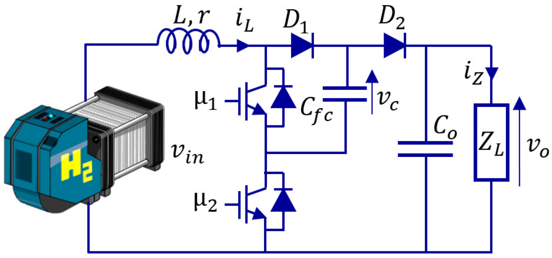

Figure 2. Three-level flying capacitor boost converter

3. CONTROLLER DESIGN

This section is devoted to the synthesis of a non-linear state feedback controller to simultaneously achieve the above-mentioned objectives. The controller to be developed has a cascade structure with nested loops. The inner control laws regulate the voltage x_2 of the floating capacitor and the current x_1 at the converter input. The external control law guarantees the regulation of the output voltage. Direct regulation of this latter is not possible, as the system has unstable zero dynamics.

3.1. Inner regulator

The internal regulator consists of two control laws. The first regulates the voltage of the floating capacitor to reduce voltage stress on the semi-conductors, while the second regulates the fuel cell's current output to avoid the problem of unstable zero dynamics. Both control subsystems exhibit initial coupling, which will be addressed by decoupling in the regulator to be developed.

3.1.1. Fuel cell's current control

Due to the non-minimum phase characteristics of the system, the output voltage x_3 is indirectly regulated by controlling the current x_1. The controller is made up of two nested loops; An inner control loop is used to regulate the current x_1, while an outer control loop is established to achieve the regulation of the output voltage x_3 and to provide a current reference x_1^*. Based on subsystem (1), an error between current x_1 and its reference x_1^* can be defined as $z_1 = L\left(x_1 - x_1^*\right)$. Using subsystem (1), the dynamics of z_L is given as (4).

$$\dot{z}_1 = v_{in} + \left(u_1 - u_2\right) x_2 - \left(1 - u_2\right)\ x_3 - r x_1 - L\dot{x}_1^* \tag{4}$$

To guaranty the asymptotic stability of the system one defined a positive Lyapunov function $v_2 = \frac{1}{2}z_1^2$, it's dynamic is given by (5).

$$\dot{v}_2 = z_1\left(v_{in} + \left(u_1 - u_2\right)\ x_2 - \left(1 - u_2\right)\ x_3 - r x_1 - L\dot{x}_1^*\right) \tag{5}$$

To make the Lyapunov function dynamics negative, one chooses the (6).

$$v_{in} + \left(u_1 - u_2\right)\ x_2 - \left(1 - u_2\right)\ x_3 - r x_1 - L\dot{x}_1^* = -k_L z_1 \tag{6}$$

With k_L is a positive design parameter. Rewriting (6), the input control u_2 is given by the (7).

$$u_2 = \frac{1}{x_3 - x_2}\left(x_3 - v_{in} - u_1 x_2\ + r\ x_1 + L\dot{x}_1^* - k_L\ z_1\right) \tag{7}$$

Hence, in (4) and (5) become: $\dot{z}_1 = -k_L z_1$ and $\dot{v}_1 = -k_L z_1^2 < 0$.

3.1.2. Flying capacitor voltage regulation

For the FCBC to work correctly, it is crucial to maintain the voltage across FC at half of the output voltage x_3, regardless of the operating conditions of the system. Therefore, Lyapunov's theorem is used to design the output voltage controller x_2. Taking the tracking error as the difference between the actual signal x_2 and the desired reference $x_2^* = \dfrac{x_1}{2}$.

$$z_2 = C\left(x_2 - x_2^*\right) \tag{8}$$

Using the subsystem (2), the error dynamics z_c can be expressed as (9).

$$\dot{z}_2 = -\left(u_1 - u_2\right)\, x_1 - C\dot{x}_2^* \tag{9}$$

Regarding the Lyapunov function $v_1 = \frac{1}{2}z_2^2$ and its derivative $\dot{v}_1 = z_2\dot{z}_2$, the choice $\dot{z}_2 = -K_C\, z_2$, makes the Lyapunov function v_1 to be negative as given by (10).

$$\dot{v}_1 = -K_C z_2^2 \tag{10}$$

Where $K_C \,\epsilon\, \mathbb{R}^+$ is the adjustment parameter. Replacing the dynamic of z_2 by its expression, the control law u_1 for the subsystem (2) is constructed as (11).

$$u_1 \;= \frac{1}{x_1}\left(K_C z_2 - C\dot{x}_2^*\right) + u_2 \tag{11}$$

Solving the system of equations formed by (7) and (11) leads to the control laws (12) and (13).

$$u_1 \;= 1 + \left(K_C z_2 - C\dot{x}_2^*\right)\left(\frac{x_3 - x_2}{x_1 x_3}\right) + \frac{1}{x_3}\left(r\, x_1 - v_{in} \;+ L\,\dot{x}_1^* - k_L\, z_1\right) \tag{12}$$

$$u_2 = 1 + \frac{1}{x_3}\left(-v_{in} - \frac{x_2}{x_1}\left(K_C z_2 - C\dot{x}_2^*\right) \;+ r\, x_1 + L\,\dot{x}_1^* - k_L\, z_1\right) \tag{13}$$

3.2. Outer voltage regulator

The purpose of this loop is to force the squared output voltage to track a desired signal ${x_3^*}^2$. To achieve this, a PI-type regulator is used. Its output will serve as the reference signal for the inner loop. Assumption 1:

i) It is assumed that the state variables x_1 and x_2 exhibit faster dynamics compared to x_3. Consequently, they will quickly reach their respective reference values x_1^* and $x_2^* = \frac{x_3}{2}$, leading to the convergence of errors (z_1, z_2) to zero;

ii) The dynamics of the state variables x_1 and x_2 are assumed to be negligible, implying that $u_1 = u_2$; and

iii) The parasitic parameter r is assumed to be small.

To design this loop, a relationship is established between the DC output voltage x_3 and the virtual control input x_1^*. By substituting the control law u_2 from (11) into (3) and considering Assumption 1, one gets (14).

$$\frac{C_o}{2}\frac{dx_3^2}{dt} = -x_3 i_Z + v_{in} x_1^* \tag{14}$$

The controller input of the system (3) is chosen as (15).

$$x_1^* = \frac{\alpha\left(t\right) + x_3 i_Z}{v_{in}} \tag{15}$$

Where:

$$\alpha\left(t\right) = k_p\left(z_3 + \frac{1}{\tau_i} z_4\right) \tag{16}$$

is a signal given by the PI-controller. With in (17) and (18).

$$z_3 = \left(x_3^*\right)^2 - x_3^2 \tag{17}$$

$$z_4 = \int z_3 d\tau \tag{18}$$

The closed loop transfer function of the system (23) is given by (19).

$$H(p) = \frac{1+\tau_i p}{1+\tau_i p + \frac{\tau_i C_o}{2k_p} p^2} \tag{19}$$

Where τ_i, k_p are the design parameters to be determined.

Comparing the transfer function (19) with the standard second-order transfer function, the PI parameters can be obtained as:

$$\tau_i = \frac{2m}{\omega_0}, \qquad k_p = mC_o\omega_0.$$

where m and ω_0 are the damping coefficient and natural frequency of the system, respectively. To comply with Assumption 1, the parameters m and ω_0 are selected such that the dynamics of the inner loop are twice as fast as the dynamics of the outer loop.

4. STABILITY ANALYSIS

Stability theory is fundamental to dynamical systems theory and essential for evaluating the characteristics of a closed-loop system with its controller. Various techniques and theories exist in the literature for analyzing system stability [25], [26], including the indirect Lyapunov method and the Routh-Hurwitz criterion. Based on these theorems, we will demonstrate that the designed controllers meet the defined control objectives. The dynamic behavior of the feedback control system can be described by the state vector (20) in the $\begin{pmatrix} z_1 & z_2 & z_3 & z_4 \end{pmatrix}$ coordinates:

$$\dot{Z} = \begin{pmatrix} \dot{z}_1 & \dot{z}_2 & \dot{z}_3 & \dot{z}_4 \end{pmatrix}^T \tag{20}$$

where,

$$\dot{z}_1 = -k_L z_1\,,\, \dot{z}_2 = -K_C\, z_2, \dot{z}_3 = -c_1\, z_1 + c_2\, z_2 + \, c_3 z_3 + c_4 z_4 - c_5\, z_1^2 + c_6\, z_2^2\, - c_7 - \dot{x}_3^2, \dot{z}_4 = z_3$$

and

$c_1 = -2\left(\frac{v_{in}}{LC_o} - \frac{2rx_1^*}{LC_o} + \frac{k_L x_1^*}{C_o}\right)$, $c_2 = \frac{2K_C x_2^*}{C_o}$, $c_3 = \frac{2k_p}{C_o}$, $c_4 = \frac{2k_p}{C_o \tau_i}$, $c_5 = -2\left(-\frac{r}{C_o L^2} + \frac{k_L}{C_o L}\right)$, $c_6 = \frac{2K_C}{CC_o}$, $c_7 = \frac{2r}{C_o} x_1^{*2}$

The system (20) is nonlinear and has the equilibrium points given by (21).

$$Z_0 = \begin{pmatrix} 0 & 0 & 0 & \frac{\tau_i r}{k_p} x_1^{*2} \end{pmatrix}^T \tag{21}$$

To analyze the stability of the equilibrium Z_0 indirect Lyapunov technique have been used [27]. This involves checking whether the Jacobian matrix (22) of the state model (20), at Z_0 is Hurwitz.

$$J = \begin{pmatrix} -c_2 & 0 & 0 & 0 \\ 0 & -c_1 & 0 & 0 \\ c_1 & -c_2 & -c_3 & -c_4 \\ 0 & 0 & 1 & 0 \end{pmatrix} \tag{22}$$

The equilibrium Z_0 will be asymptotically stable if the Jacobian matrix (22) is Hurwitz. This requires proving that the real part of the eigenvalues of the following characteristic equation is negative $Re\,(\lambda_i) < 0$ [26]:

$$\pi_J = \lambda^4 + a_0\,\lambda^3 + a_1\,\lambda^2 + a_2\,\lambda + a_3 \tag{23}$$

where,

$$a_0 = c_1 + c_2 + \frac{2k_p}{C_o}, a_1 = c_1 c_2 + \frac{2k_p c_2}{C_o} + \frac{2k_p}{C_o \tau_i} + \frac{2k_p c_1}{C_o}\; a_2 = \frac{2k_p K_C}{C_o \tau_i} + \frac{2k_p k_L K_C}{C_o} + \frac{2k_p k_L}{C_o \tau_i}, a_3 = \frac{2k_p\, K_C\, k_L}{C_o \tau_i}$$

Using Routh's algebraic criterion, it appears that all zeros of the characteristic polynomial in (23) have negative real parts if the following conditions ($\frac{a_0 a_1 - a_2}{a_0} > 0$, $\frac{a_0(a_1 a_2 - a_0 a_3)}{a_0 a_1 - a_2} > 0$, $a_3 > 0$) are satisfied. Given these conditions, the matrix J is a Hurwitz matrix. According to the indirect Lyapunov method, the equilibrium Z_0 of the system (29) is asymptotically stable.

5. SIMULATION RESULTS

The controller performance was validated through simulations of the power system and the control unit, as illustrated in Figure 3 using MATLAB-Simulink. The parameters for the entire system used in the simulation are provided in Tables 1 and 2. Three test protocols were employed for the simulation:

i) Normal operation mode: Initially, the system's performance was evaluated under normal operating conditions, assuming no changes to the overall system parameters;

ii) Output voltage reference Variation: In the second test, a variation in the output voltage reference was introduced to assess the system's response to changes in the desired output voltage; and

iii) Load variation: In the final test, a load variation was applied to evaluate the robustness of the system.

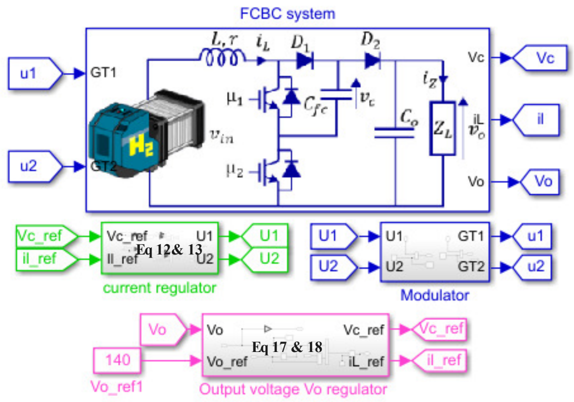

Figure 3. System structure in MATLAB/Simulink

Table 1. System parameters

Item	Symbol	Value	Unit
DC source	E	100	V
Current inductance	L	500	H
Parasitic resistance	r	2	Ω
Floating capacitor	C_{fc}	100	μF
Output capacitor	C_o	100	μF
Load	R	40	Ω
Switching frequency	f_{sw}	20	kHz

Table 2. Controller parameters

Item	Symbol	Value	Unit
PI coefficients	ω_0	312	rad/s
	m	4	–
	K_p	0.833	$mA.V^{-2}$
	τ_i	0.833	$A.V^{-2}.s^{-1}$
Output voltage regulator coefficient	k_L	18000	–
Floating capacitor voltage regulator coefficient	k_c	18000	–
Routh Hurwitz coefficients	a_0	66100	–
	a_1	1.0706×10^9	–
	a_2	1.0706×10^{11}	–
	a_3	1.0640×10^{13}	–

5.1. Operation under normal mode

The system's response in normal operation is depicted in Figures 4–6. These figures illustrate that the inductance current i_L, flying capacitor voltage v_c and the output voltage v_o, are well regulated to their reference values. Where, Figure 4 shows the inductance current tracking its reference value with minimal deviation, indicating that the inner control loop effectively maintains the desired current level. This precise control ensures that the current supplied to the load remains stable, contributing to the overall stability of the power system. Figure 5 shows the voltage across the flying capacitor. The plot demonstrates that the flying capacitor voltage is consistently regulated, reflecting the controller's ability to manage the voltage stress on the semiconductors effectively. Proper regulation of the flying capacitor voltage is crucial for the longevity and reliability of the power-electronic components within the system. Figure 6 highlights the output voltage v_o, showing its stable tracking of the reference voltage.

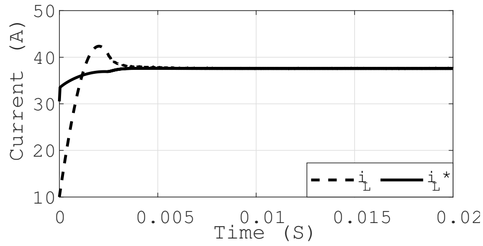

Figure 4. Inductance current i_L and its reference

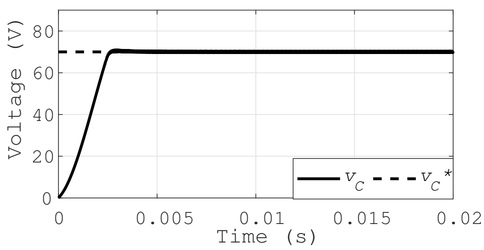

Figure 5. FC voltage v_c and its reference

5.2. Robustness tests under parameter output voltage reference variation

Figures 7–9 show the simulation results for a step change in the reference output voltage v_o. The reference voltage is altered from 100 V to 140 V at time $t_1 = 20\ ms$ and from 140 V back to 100 V at $t_2 = 40\ ms$. Despite these abrupt changes, the figures demonstrate that the signals i_L, v_c and v_o closely follow their respective reference values, Figure 7 illustrates the response of the inductance current i_L, which adapts rapidly to the new reference values. The control system effectively manages the transition, ensuring that the current remains stable and within the desired range. This rapid adjustment indicates the inner loop's robustness and its ability to handle sudden changes without significant overshot or oscillation. Figure 8 shows the voltage across the flying capacitor v_c. The plot reveals that the flying capacitor voltage quickly stabilizes after each change in the reference output voltage, highlighting the controller's efficiency in managing voltage stress. This capability is crucial for maintaining the reliability of the power electronic components, as it prevents excessive voltage variations that could potentially harm the system. Figure 9 focuses on the output voltage v_o, demonstrating its precise tracking of the reference voltage throughout the changes. The controller successfully adjusts the output voltage to the new reference values with minimal delay.

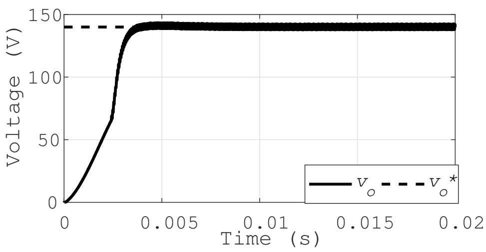

Figure 6. Output voltage v_o and its reference

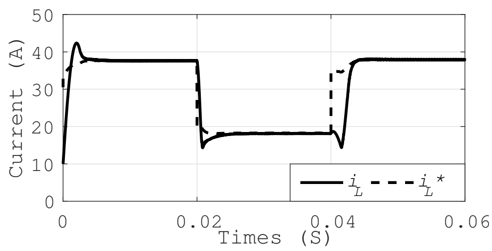

Figure 7. Inductance current i_L and its reference

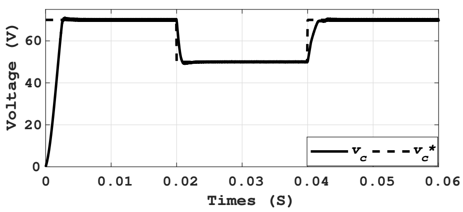

Figure 8. FC voltage v_c and its reference

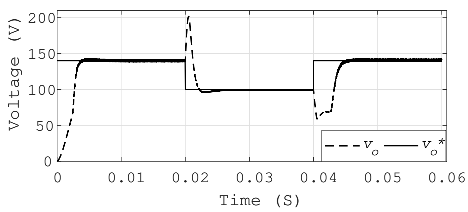

Figure 9. FC voltage v_c and its reference

5.3. Robustness tests under load variation

In the third test, the load undergoes variation from $40\,\Omega$ to $20\,\Omega$ at $t_1 = 20\,ms$ and from $20\,\Omega$ to $10\,\Omega$ at the time $t_2 = 40\,ms$. The results of the test are shown in Figures 10 and 11. These figures demonstrate that the proposed controller successfully maintains the inductance current i_L and the output voltage v_c at their reference values despite the significant change in resistive load. Figure 10 displays the response of the inductance current i_L. Even with the sudden decrease in load resistance, the inductance current closely follows its reference value, showcasing the controller's ability to adapt to changes in the load. Figure 11 shows the flying capacitor voltage v_c. The plot indicates that v_c stays balanced despite the changes in load resistance, highlighting the controller's capability to maintain voltage stability across the flying capacitor.

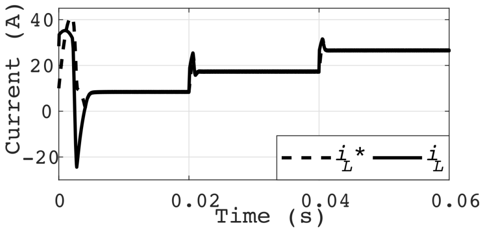

Figure 10. Inductance current i_L and its reference under parameter variations

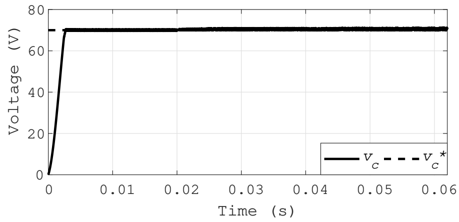

Figure 11. FC voltage v_c and its reference under parameter variations

6. CONCLUSION

This work presents the control of a three-level flying capacitor boost converter integrated into a hybrid electric vehicle powered by a fuel cell. The proposed controller features an internal loop designed to regulate the input current and balance the floating capacitor voltage, developed using the Lyapunov technique. Additionally, an external loop regulates the output voltage and provides a suitable reference for the inductor current. The stability analysis conducted in this work has verified that the control objectives are effectively achieved. Simulation results have validated the controllers robustness against load variations and changes in the output voltage reference, these findings corroborate the theoretical results and demonstrate the practical effectiveness of the proposed control strategy. In conclusion, the developed controller improves the operational stability and efficiency of the three-level flying capacitor boost converter in a hybrid electric vehicle context. The study contributes valuable insights into advanced control techniques for power electronics applications, paving the way for further advancements in hybrid vehicle technologies.

FUNDING INFORMATION

This research received no external funding.

AUTHOR CONTRIBUTIONS STATEMENT

This journal uses the Contributor Roles Taxonomy (CRediT) to recognize individual author contributions, reduce authorship disputes, and facilitate collaboration.

Name of Author	C	M	So	Va	Fo	I	R	D	O	E	Vi	Su	P	Fu
Chaouqi Aouadi	✓	✓	✓		✓	✓			✓	✓	✓			
Abdelmajid Abouloifa	✓	✓			✓	✓			✓	✓		✓		
Meriem Aourir		✓	✓			✓			✓	✓				
Ibtissam Lachkar		✓				✓			✓			✓		

C	: **C**onceptualization	I	: **I**nvestigation	Vi	: **Vi**sualization
M	: **M**ethodology	R	: **R**esources	Su	: **Su**pervision
So	: **So**ftware	D	: **D**ata Curation	P	: **P**roject Administration
Va	: **Va**lidation	O	: Writing - **O**riginal Draft	Fu	: **Fu**nding Acquisition
Fo	: **Fo**rmal Analysis	E	: Writing - Review & **E**diting		

CONFLICT OF INTEREST STATEMENT

The authors declare no conflict of interest.

DATA AVAILABILITY

Data supporting the findings of this study are available in the article. More information is available from the corresponding authors upon reasonable request.

REFERENCES

[1] Q. Xu, W. Jiang, F. Blaabjerg, C. Zhang, X. Zhang, and T. Fernando, "Backstepping control for large signal stability of high boost ratio interleaved converter interfaced DC microgrids with constant power loads," *IEEE Transactions on Power Electronics*, vol. 35, no. 5, pp. 5397–5407, May 2020, doi: 10.1109/TPEL.2019.2943889.

[2] Y.-C. Jeung, D. D. Le, and D.-C. Lee, "Analysis and design of DC-bus voltage controller of energy storage systems in dc microgrids," *IEEE Access*, vol. 7, pp. 126696–126708, 2019, doi: 10.1109/ACCESS.2019.2939176.

[3] M. Aourir, A. Abouloifa, I. Lachkar, C. Aouadi, F. Giri, and J. M. Guerrero, "Nonlinear control and stability analysis of single stage grid-connected photovoltaic systems," *International Journal of Electrical Power and Energy Systems*, vol. 115, p. 105439, Feb. 2020, doi: 10.1016/j.ijepes.2019.105439.

[4] P. K. Maroti, S. Padmanaban, M. S. Bhaskar, V. K. Ramachandaramurthy, and F. Blaabjerg, "The state-of-the-art of power electronics converters configurations in electric vehicle technologies," *Power Electronic Devices and Components*, vol. 1, p. 100001, Mar. 2022, doi: 10.1016/j.pedc.2021.100001.

[5] H. Komurcugil and O. Kukrer, "A new control strategy for single-phase shunt active power filters using a Lyapunov function," *IEEE Transactions on Industrial Electronics*, vol. 53, no. 1, pp. 305–312, Feb. 2006, doi: 10.1109/TIE.2005.862218.

[6] Z. Hekss, A. Abouloifa, S. Echalih, I. Lachkar, A. El Aroudi, and F. Giri, "Flatness based control of single phase grid connected photovoltaic system associated with a shunt active power filter," *IFAC-PapersOnLine*, vol. 55, no. 12, pp. 43–48, 2022, doi: 10.1016/j.ifacol.2022.07.286.

[7] K. Bi, Y. Lu, Y. Zhuang, Y. Zhu, and Q. Fan, "Decoupling power balancing strategy with reduced current sensors for two-phase interleaved neutral point clamped DC/DC converter applied in energy storage system," *IEEE Transactions on Energy Conversion*, vol. 38, no. 1, pp. 147–157, Mar. 2023, doi: 10.1109/TEC.2022.3190309.

[8] M. Kissaoui, A. Abouloifa, Y. Abouelmahjoub, F. Z. Chaoui, and F. Giri, "Output-feedback nonlinear adaptive control of single-phase half-bridge UPS systems," *Asian Journal of Control*, vol. 18, no. 6, pp. 1995–2009, Nov. 2016, doi: 10.1002/asjc.1293.

[9] K. Bi *et al.*, "A model predictive controlled bidirectional four quadrant flying capacitor DC/DC converter applied in energy storage system," *IEEE Transactions on Power Electronics*, vol. 37, no. 7, pp. 7705–7717, Jul. 2022, doi: 10.1109/TPEL.2022.3146510.

[10] S. Nady, H. El Fadil, Z. El Idrissi, A. Lassioui, A. Intidam, and H. Anwar, "Development and experimental validation of high-order sliding mode control for quadratic boost converters in fuel cell electric vehicles," *Scientific African*, vol. 26, p. e02417, Dec. 2024, doi: 10.1016/j.sciaf.2024.e02417.

[11] M. T. Zhang, Yimin Jiang, F. C. Lee, and M. M. Jovanovic, "Single-phase three-level boost power factor correction converter," in *Proceedings of 1995 IEEE Applied Power Electronics Conference and Exposition - APEC'95*, IEEE, 1995, pp. 434–439 vol.1. doi: 10.1109/APEC.1995.468984.

[12] W. Li, Y. Zhao, J. Wu, and X. He, "Interleaved high step-up converter with winding-cross-coupled inductors and voltage multiplier cells," *IEEE Transactions on Power Electronics*, vol. 27, no. 1, pp. 133–143, Jan. 2012, doi: 10.1109/TPEL.2009.2028688.

[13] V. A. K. Prabhala, P. Fajri, V. S. P. Gouribhatla, B. P. Baddipadiga, and M. Ferdowsi, "A DC–DC converter with high voltage gain and two input boost stages," *IEEE Transactions on Power Electronics*, vol. 31, no. 6, pp. 4206–4215, Jun. 2016, doi: 10.1109/TPEL.2015.2476377.

[14] Y. Zhang, J.-T. Sun, and Y.-F. Wang, "Hybrid boost three-level dc–dc converter with high voltage gain for photovoltaic generation systems," *IEEE Transactions on Power Electronics*, vol. 28, no. 8, pp. 3659–3664, Aug. 2013, doi: 10.1109/TPEL.2012.2229720.

[15] X. Ge, D. Xiao, Y. Lu, and W. Luo, "Adaptive sliding mode control for interleaved nx multilevel boost converter," *IEEE Access*, vol. 11, pp. 27843–27852, 2023, doi: 10.1109/ACCESS.2023.3257997.

[16] R. Garnayak, P. Majumder, S. Kapat, and C. Chakraborty, "A hybrid design framework for fast transient and voltage balancing in a three-level flying capacitor boost converter with digital current mode control," *IEEE Transactions on Power Electronics*, vol. 38, no. 11, pp. 13674–13685, Nov. 2023, doi: 10.1109/TPEL.2023.3293829.

[17] H.-C. Chen, C.-Y. Lu, W.-H. Lien, and T.-H. Chen, "Active capacitor voltage balancing control for three-level flying capacitor boost converter based on average-behavior circuit model," *IEEE Transactions on Industry Applications*, vol. 55, no. 2, pp. 1628–1638, Mar. 2019, doi: 10.1109/TIA.2018.2876031.

[18] H. Keyhani and H. A. Toliyat, "Flying-capacitor boost converter," in *2012 Twenty-Seventh Annual IEEE Applied Power Electronics Conference and Exposition (APEC)*, IEEE, Feb. 2012, pp. 2311–2318. doi: 10.1109/APEC.2012.6166145.

[19] H. Chen, D. Wang, S. Tang, X. Yin, J. Wang, and Z. J. Shen, "Continuous control set model predictive control for three-level flying capacitor boost converter with constant switching frequency," *IEEE Journal of Emerging and Selected Topics in Power Electronics*, vol. 9, no. 5, pp. 5996–6007, Oct. 2021, doi: 10.1109/JESTPE.2020.3044963.

[20] V. Jayan, A. Ghias, and A. Merabet, "Fixed frequency model predictive control of three-level bi-directional flying capacitor dc-dc converter in DC microgrid," in *IECON 2019 - 45th Annual Conference of the IEEE Industrial Electronics Society*, IEEE, Oct. 2019, pp. 3343–3348. doi: 10.1109/IECON.2019.8927435.

[21] A. Shukla, A. Ghosh, and A. Joshi, "Improved multilevel hysteresis current regulation and capacitor voltage balancing schemes for flying capacitor multilevel inverter," *IEEE Transactions on Power Electronics*, vol. 23, no. 2, pp. 518–529, Mar. 2008, doi: 10.1109/TPEL.2007.915788.

[22] B. P. McGrath and D. G. Holmes, "Analytical modelling of voltage balance dynamics for a flying capacitor multilevel converter," *IEEE Transactions on Power Electronics*, vol. 23, no. 2, pp. 543–550, Mar. 2008, doi: 10.1109/TPEL.2007.915175.

[23] C. Feng, J. Liang, and V. G. Agelidis, "Modified phase-shifted PWM control for flying capacitor multilevel converters," *IEEE Transactions on Power Electronics*, vol. 22, no. 1, pp. 178–185, Jan. 2007, doi: 10.1109/TPEL.2006.886600.

[24] A. B. Aher, S. M. Patil, and T. Sutikno, "Design and development of model for proton exchange membrane fuel cell," *International Journal of Power Electronics and Drive Systems*, vol. 15, no. 2, pp. 1061–1071, 2024, doi: 10.11591/ijpeds.v15.i2.pp1061-1071.

[25] C. Wang, M. H. Nehrir, and S. Shaw, "Dynamic models and model validation for pem fuel cells using electrical circuits," in *IEEE Power Engineering Society General Meeting*, 2005, IEEE, 2005, pp. 1000–1000. doi: 10.1109/PES.2005.1489284.

[26] H. K. Khalil, *Nonlinear control*. in Always Learning. Pearson, 2015. [Online]. Available: https://books.google.co.id/books?id=-WbjoAEACAAJ.

[27] G. A. Hernandez-Castorena, M. A. Alcorta-Garcia, J. A. Saenz-Esqueda, and G. M. Mendez, "Lyapunov's stability analysis for first degree polynomial systems, subject to risk-sensitive control," *Mathematics and Computers in Simulation*, vol. 226, pp. 464–473, 2024, doi: 10.1016/j.matcom.2024.07.006.

BIOGRAPHIES OF AUTHORS

Chaouqi Aouadi holds his Ph.D. degree in control engineering and renewable energies in 2018 and a Master degree in information processing in 2014 from the Faculty of Science Ben M'sick, Hassan II University. He is currently professor with the department of Electrical Engineering at National High school of electricity and Mechanics (ENSEM) at Hassan II university of Casablanca, Morocco. His research areas of interest include power converter, nonlinear control and artificial intelligent. He can be contacted at email: c.aouadi@ensem.ac.ma or chaouqi.aouadi@univh2c.ma.

Abdelmajid Abouloifa received the Aggregation of Electrical Engineering from Normal High School, Rabat, Morocco, in 1999, and Ph.D. degree in control engineering from the University of Caen Basse-Normandie, Caen, France and from Mohammed V University, Rabat, Morocco in 2008.He is currently Professor at the National High School for Electricity and mechanics (ENSEM), University Hassan II, Casablanca,Morocco. His research interests include high frequency power converter topologies, power-factor-correction techniques, power supplies, and nonlinear control. He can be contacted at email: a.abouloifa@gmail.com.

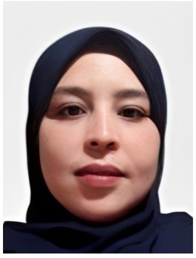

Meriem Aourir received her Ph.D. degree in in the field of automatic, renewable energy, Power electronics in 2021 and she has got master degree in information processing from Faculty of Science Ben M'sik, University of Hassan II Casablanca in 2015. Currently, she is a permanent professor in Higher Institute of engineering and busines. She can be contacted at email: meriem.aourir@gmail.com.

Ibtissam Lachkar received the graduate degree from the Normal High School of Technical Education, Rabat, Morocco, in 1995, the degree in high depth studies from the Mohammadia School of Engineers, Rabat, in 2005, and the Ph.D. degree from the Mohammadia School of Engineers. Currently, she is a professor at the National High School for Electricity and mechanics (ENSEM), Hassan II University of Casablanca. Her research interests include modeling, nonlinear control, power converters, uninterruptible power supplies, and photovoltaic systems and drones. She can be contacted at email: lachkaribtissam@gmail.com.